Glutamate Transporter-Associated Anion Channels Adjust Intracellular Chloride Concentrations during Glial Maturation

Verena Untiet,[1] Peter Kovermann,[1] Niklas J. Gerkau,[2] Thomas Gensch,[1] Christine R. Rose,[2] and Christoph Fahlke[1]

Astrocytic volume regulation and neurotransmitter uptake are critically dependent on the intracellular anion concentration, but little is known about the mechanisms controlling internal anion homeostasis in these cells. Here we used fluorescence lifetime imaging microscopy (FLIM) with the chloride-sensitive dye MQAE to measure intracellular chloride concentrations in murine Bergmann glial cells in acute cerebellar slices. We found Bergmann glial $[Cl^-]_{int}$ to be controlled by two opposing transport processes: chloride is actively accumulated by the Na^+-K^+-$2Cl^-$ cotransporter NKCC1, and chloride efflux through anion channels associated with excitatory amino acid transporters (EAATs) reduces $[Cl^-]_{int}$ to values that vary upon changes in expression levels or activity of these channels. EAATs transiently form anion-selective channels during glutamate transport, and thus represent a class of ligand-gated anion channels. Age-dependent upregulation of EAATs results in a developmental chloride switch from high internal chloride concentrations (51.6 ± 2.2 mM, mean ± 95% confidence interval) during early development to adult levels (35.3 ± 0.3 mM). Simultaneous blockade of EAAT1/GLAST and EAAT2/GLT-1 increased $[Cl^-]_{int}$ in adult glia to neonatal values. Moreover, EAAT activation by synaptic stimulations rapidly decreased $[Cl^-]_{int}$. Other tested chloride channels or chloride transporters do not contribute to $[Cl^-]_{int}$ under our experimental conditions. Neither genetic removal of ClC-2 nor pharmacological block of K^+-Cl^- cotransporter change resting Bergmann glial $[Cl^-]_{int}$ in acute cerebellar slices. We conclude that EAAT anion channels play an important and unexpected role in adjusting glial intracellular anion concentration during maturation and in response to cerebellar activity.

Key words: Bergmann glia, fluorescence lifetime imaging, glial chloride switch, EAAT

Introduction

In the central nervous system, astrocytes remove neurotransmitters from the synaptic cleft and supply nutrients and signaling molecules to neurons (Deitmer and Rose, 2010). Many of these physiological tasks are linked to transmembrane ion gradients and are therefore regulated by intra- or extracellular ion concentrations. The intracellular chloride concentration ($[Cl^-]_{int}$) determines chloride fluxes during regulatory volume changes (Mongin, 2015) and contributes to the driving force for $GABA_A$ receptor currents (MacVicar et al., 1989; Muller et al., 1994) and for various Cl^--coupled secondary active cotransporters (Zomot et al., 2007). Disturbed astrocytic anion homeostasis might thus impair neurotransmitter transport and astrocytic volume regulation, perturb normal synaptic transmission, and induce astrocytic swelling.

Despite its major physiological importance, little is known about the chloride concentrations in adult astrocytes and their dynamic adjustment during neuronal activity, as well as their potential developmental regulation. So far, glial $[Cl^-]_{int}$ has been determined in cultured astrocytes with results varying between 29–46 mM (Bekar and Walz, 2002; Bevensee et al., 1997; Kettenmann et al., 1987; Kimelberg, 1981; Smith et al., 1981; Walz and Mukerji, 1988). Here we used fluorescence lifetime imaging microscopy (FLIM) with the chloride-sensitive dye MQAE (Gensch et al., 2015; Kovalchuk and Garaschuk,

View this article online at wileyonlinelibrary.com. DOI: 10.1002/glia.23098

Published online Month 00, 2016 in Wiley Online Library (wileyonlinelibrary.com). Received June 22, 2016, Accepted for publication Oct 24, 2016.

Address correspondence to Christoph Fahlke, Institute of Complex Systems, Zelluläre Biophysik (ICS-4), Forschungszentrum Jülich, 52425 Jülich, Germany. E-mail: c.fahlke@fz-juelich.de

From the [1]Institute of Complex Systems, Zelluläre Biophysik (ICS-4), Forschungszentrum Jülich, Germany; [2]Institute of Neurobiology, Heinrich-Heine-Universität Düsseldorf, Germany

Additional Supporting Information may be found in the online version of this article.

2012; Marandi et al., 2002; Untiet et al., 2016) in acute cerebellar slices to determine the $[Cl^-]_{int}$ in Bergmann glial cells at different stages of postnatal development and to study pathways involved in its regulation. We found that anion channels associated with two glial glutamate transporters, excitatory amino acid transporter 1 and 2 (EAAT1 and EAAT2), modify the resting $[Cl^-]_{int}$ in adult wild type (WT) glia and dynamically modulate these values in response to cerebellar neuronal activity. The developmental upregulation of these transporters induces a significant decrease in $[Cl^-]_{int}$ during glial maturation.

Materials and Methods

Animals

Animals were housed under standard conditions in the animal facility of the Forschungszentrum Jülich according to institutional guidelines under a 12-h light/dark cycle. All experiments are in compliance with the German Law for Protection of Animals (Reference number 84-02.04.2014.A334) and were approved by the regulatory authorities, the Forschungszentrum Jülich, and the Landesamt für Natur, Umwelt und Verbraucherschutz of Nordrhein-Westfalen.

Preparation of Acute Cerebellar Slices

After anesthetizing animals with isoflurane and decapitation, the brains were rapidly removed and placed in ice-cold Ringer's solution (125 mM NaCl, 2.5 mM KCl, 1.25 mM NaH_2PO_4, 26 mM $NaHCO_3$, 0.5 mM $CaCl_2$, 5 mM $MgCl_2$, 20 mM glucose) for preparation. Sagittal cerebellar slices (250 μm thick) were cut at 4°C with a Microm HM650V (Thermo Scientific, Walldorf, Germany; frequency 60 Hz, amplitude 1 mm, drive 10) and transferred for 30 min to a gauze slice holder in oxygenated Ringer's solution at 37°C (Bennay et al., 2008). Cerebellar slices were then placed in standard oxygenated Ringer's solution (125 mM NaCl, 2.5 mM KCl, 1.25 mM NaH_2PO_4, 26 mM $NaHCO_3$, 2 mM $CaCl_2$, 1 mM $MgCl_2$, 25 mM glucose) and stored at room temperature (20°C −22°C) for at least 90 min. Slices were constantly perfused with oxygenated (carbogen; 5% CO_2 in O_2) standard Ringer's solution, and all measurements were completed within 8 h of brain removal. All blockade experiments (Figs. 2, 3, and 5) were performed using mice aged P20–P30, unless stated otherwise. UCPH-101 (Abcam, Cambridge, UK) has very slow unblocking kinetics (Abrahamsen et al., 2013) and is not washed out within the measurement period (around 15 min). Hence, for UCPH-101 experiments, slices were incubated with this blocker for 10 min before use and then perfused with standard Ringer's solution without additional blocker during chloride imaging. All other blockers were added to both the incubation solution and the perfusion solution. For blocking EAATs, we used either DL-TBOA or TFB-TBOA, which were reported to have similar properties (Shimamoto et al., 2004).

Fluorescence Lifetime Imaging Microscopy (FLIM)

Prior to chloride imaging experiments, cerebellar slices were incubated in oxygenated standard Ringer's solution containing 3.5 mM 1-(ethoxycarbonylmethyl)−6-methoxyquinolinium bromide (MQAE; Sigma-Aldrich, Munich, Germany; Verkman, 1990) for 30 min at room temperature. After transfer to an imaging chamber placed on the stage of an upright fluorescence microscope (A1 MP; Nikon, Amsterdam, The Netherlands) equipped with a 25 × water immersion objective (NA1.1; WD 2 mm; XYZ, Nikon), fluorescence was stimulated by 100 fs light pulses ($\lambda_{exc} = 750$ nm) by two-photon excitation. Laser pulses were generated at a frequency of 80 MHz by a mode-locked Titan-Sapphire laser (Mai Tai DeepSee, Newport Spectra Physics; Irvine, CA; output power 2.3 W at 750 nm). Mean fluorescence lifetimes were measured using multidimensional time-correlated single photon counting (TCSPC) in a volume of 0.08 μm^3 per individual pixel. We obtained a three-dimensional resolution of approximately 1 μm in the *z*-axis and 0.3 μm in the *x*- and *y*-axes.

Laser light was directed onto the cerebellar slice through the lens with a reduced power of around 5 mW at the sample. Fluorescence was filtered by separating MQAE fluorescence (emission 460 nm) from autofluorescence (short pass filter, 500 nm, $\lambda_{obs} <$ 510 nm; Omega Optical, Brattleboro, VT) and recorded with a GaAsP hybrid photodetector (HPM-100-40; Becker & Hickl, Berlin, Germany). TCSPC electronics (SPC-152; Becker & Hickl), and acquisition software were used for fluorescence lifetime imaging as previously described (Kaneko et al., 2004). Lifetime images were analyzed using SPCImage 4.8 (Becker & Hickl) with a bin of 5 by fitting a bi-exponential function to the fluorescence decay. Due to the small dimensions of glial processes (Grosche et al., 1999) we were unable to unambiguously distinguish them from those of neighboring dendrites, preventing accurate calibration and fluorescence lifetime measurements. We therefore restricted our analysis to Bergmann glial somata.

Electrical stimulation of parallel fibers was performed by square pulses (150 μs duration, 10 mA) delivered at 200 Hz via a bipolar electrode (PI2CEA3 concentric bipolar electrode, tip diameter 2–3 μm, platinum/iridium; Science Products, Hofheim, Germany) positioned in the molecular layer. Trains of 20 pulses were applied every 10 s over a period of 1 min. Somata of single cells within a distance of 60–135 μm from the electrode were analyzed.

For chloride concentration calibration (Figs. 1C and Supp. Info. Fig. S1), cerebellar slices were incubated in HEPES-buffered solution (140 mM K^+, 10 mM Na^+, 10 mM HEPES, 4–140 mM Cl^-, 10–150 mM gluconate, adjusted to 310 mOsmol/L with K–gluconate and to pH 7.4 with KOH) containing 10 μM nigericin (sodium salt; Sigma-Aldrich, Munich, Germany) and 10 μM tributyltin (chloride salt; Sigma-Aldrich; Bevensee et al., 1997; Chao et al., 1989; Kaneko et al., 2004). Since quenching of MQAE fluorescence by HCO_3^- is much less effective than by Cl^-(Kaneko et al., 2004), intracellular bicarbonate is not expected to contribute to the MQAE lifetime and was therefore ignored in calibration experiments. Fluorescence lifetimes were measured for multiple cells for $[Cl^-]_{ext}$ (20, 22, 26, 30, 34, 38, 40, 44, 60, 80, and 140 mM) and the inverse fluorescence lifetime ($1/\tau$) was plotted against $[Cl^-]$ (Fig. 1C). Most average fluorescence lifetimes determined for different preset chloride concentrations, especially in the physiological rage determined for Bergmann glia (34 to 40 mM), were significantly different (Fig. 1C, Supp. Info. Table 1). A least square fit of a linear function to these data provides the calibration curve. For all experimentally determined fluorescence lifetimes, the corresponding

chloride concentrations were determined using this calibration curve. To determine $K_{SV,}$ τ_0 was determined as the inverse of the intercept of the calibration curve. The product of τ_0 and the slope of the calibration curve yields K_{SV}.

All chloride concentrations are given as mean values for all cells measured under the same conditions ± the 95% confidence intervals. For each measurement, three to four images were taken per slice at the third to fifth Bergmann glial cell layer from the upper cutting edge. All cells that could be identified as Bergmann glial cells based on their characteristic morphology (cell size and location between Purkinje cells) and that were sufficiently loaded with MQAE were analyzed. Each glial soma was defined as a region of interest (ROI), and fluorescence lifetimes were determined as mean values of the average fluorescence lifetimes of all pixels in a given ROI. Prior to every blockade experiment (Figs. 2, 3, and 5, and Supp. Info. Fig. S2), at least two slices were measured under physiological conditions. For stimulation experiments (Fig. 5), the resting $[Cl^-]_{int}$ was measured twice before pulse application. All measurements in which the slices moved in the *x*, *y*, or *z* direction were excluded from the analysis. For electrical stimulations, only cells that could be identified before and after the stimulation were analyzed.

Na^+ Imaging

Wide-field fluorescence imaging was performed as previously described (Langer and Rose, 2009; Rose and Ransom, 1996) using a four-dimensional digital imaging system controlled by Nikon NIS-Elements v4.3 software (Nikon) and an upright microscope (Nikon Eclipse FN-PT) equipped with 40×/N.A. 0.8 LUMPlanFI water immersion objective (Olympus, Hamburg, Germany) and an Orca FLASH-IV V2 camera (Hamamatsu Photonics, Herrsching, Germany). For sodium imaging, cerebellar slices were stained by a bolus injection of membrane-permeable sodium-binding benzofuran isophthalate-acetoxymethyl ester (SBFI-AM; Invitrogen, Karlsruhe, Germany). Cells were excited at 380 nm and fluorescence emission (> 440 nm) was measured at 0.5 Hz from defined regions of interest representing the somata of Bergmann glial cells. Standard dynamic background correction was performed as previously described (Langer and Rose, 2009). Data were analyzed off-line using Origin 9.0 Software (OriginLab, Northampton, MA). SBFI fluorescence was calibrated *in situ* as previously reported (Langer and Rose, 2009; Rose and Ransom, 1996).

Changes in sodium concentration relative to baseline are given as the mean of all cells measured under the same conditions ± 95% confidence intervals. For each measurement, all cells that could be identified as Bergmann glial cells and were sufficiently loaded with SBFI were analyzed. Prior to the application of blockers, baseline sodium was recorded for at least 10 min under physiological conditions.

Western Blot Analysis

Animals were killed by decapitation after anesthetizing with isoflurane. The cerebellums were rapidly removed, snap frozen in liquid nitrogen, and homogenized in cold lysis buffer (at 4°C; 1 mM EDTA, 10 mM Tris-Cl (pH 7.4), 0.1 mM DTT). The homogenate was clarified at 3,000 *g* for 5 min and the resulting supernatant was centrifuged at 100,000 *g* for 45 min. The pellet was resuspended in 100 µL solubilizing buffer (1 mM EDTA, 50 mM Tris-Cl (pH 7.4), 1% (v/v) Triton X-100, 0.5% (w/v) SDS, 2 µL/mL protease inhibitor). Proteins were separated by SDS-PAGE and blotted onto nitrocellulose. Blots were washed with Tris-buffered saline, blocked and incubated for 1 h at room temperature with primary antibodies against EAAT1/GLAST (1:1,000 Miltenyi Biotec, Bergisch Gladbach, Germany), EAAT2/GLT-1 (1:2,000; Chemicon, Temecula, CA), or actin (1:2,000; Sigma-Aldrich). Membranes were washed and incubated with horseradish peroxidase conjugated secondary antibody (Thermo Scientific; 1:25,000) for 1 h at room temperature for immunodetection. Protein bands were visualized via chemiluminescence.

Statistical Analysis

All data represent mean values ± 95% confidence intervals or SEM. The mean chloride concentrations were obtained from measured fluorescence lifetimes using the calibration curve obtained from permeabilized Bergmann glial cells (Fig. 1C). The standard deviations of $[Cl^-]_{int}$ were calculated using error propagation (Ku, 1996).

$$\sigma_{Cl^-} = \sqrt{\left(\alpha * \frac{1}{\tau}\right)^2 * \left(\frac{\sigma_\alpha^2}{\alpha^2} + \frac{\sigma_\tau^2}{\tau^2}\right) + \sigma_\beta^2}$$

with α being the slope of the calibration curve, σ_α being the standard deviation of α, β being the intercept of the calibration curve with the *y*-axis and σ_β its standard deviation. τ gives the mean value of all measured fluorescence lifetimes for each condition, and σ_τ its standard deviation. Confidence intervals were calculated as standard deviations divided by the square root of the number of investigated cells (*n*) multiplied with 1.96.

$$95\,\%\,\text{confidence interval}\,(A) = \bar{Cl}_A^- \pm 1.96 * \left(\frac{\sigma_{Cl_A^-}}{\sqrt{n_A}}\right)$$

Statistical analysis of chloride concentrations was performed by a two-tailed Students *t*-test considering the propagated variance of the compared experiments:

$$\sigma^2 = \frac{\left[(n-1)\sigma_A^2\right] + \left[(m-1)\sigma_B^2\right]}{n+m-2}$$

$$T = \frac{\left(\bar{A} - \bar{B}\right)}{\sigma\sqrt{\left(\frac{1}{n}\right) - \left(\frac{1}{m}\right)}}$$

p-values were calculated from *T*-values using Excel and $p = T.VERT.2S(\mathrm{T};(m+n-2))$.

Statistical analysis of sodium concentrations was performed using the two-tailed Student's *t*-test (for normal distribution) or Mann–Whitney rank sum test. Asterisks indicate the level of significance (***$p < 0.001$, ** $p < 0.01$, * $p < 0.05$).

Results

Determination of $[Cl^-]_{int}$ in Bergmann Glial Cells

To determine $[Cl^-]_{int}$ in Bergmann glial cells, we prepared acute cerebellar slices and loaded them with the chloride-sensitive fluorescent dye 1-(ethoxycarbonylmethyl)-6-methoxyquinolinium bromide (MQAE). Cl^- ions reduce both the fluorescence intensity and fluorescence lifetime of MQAE by collisional quenching, resulting in an inverse linear

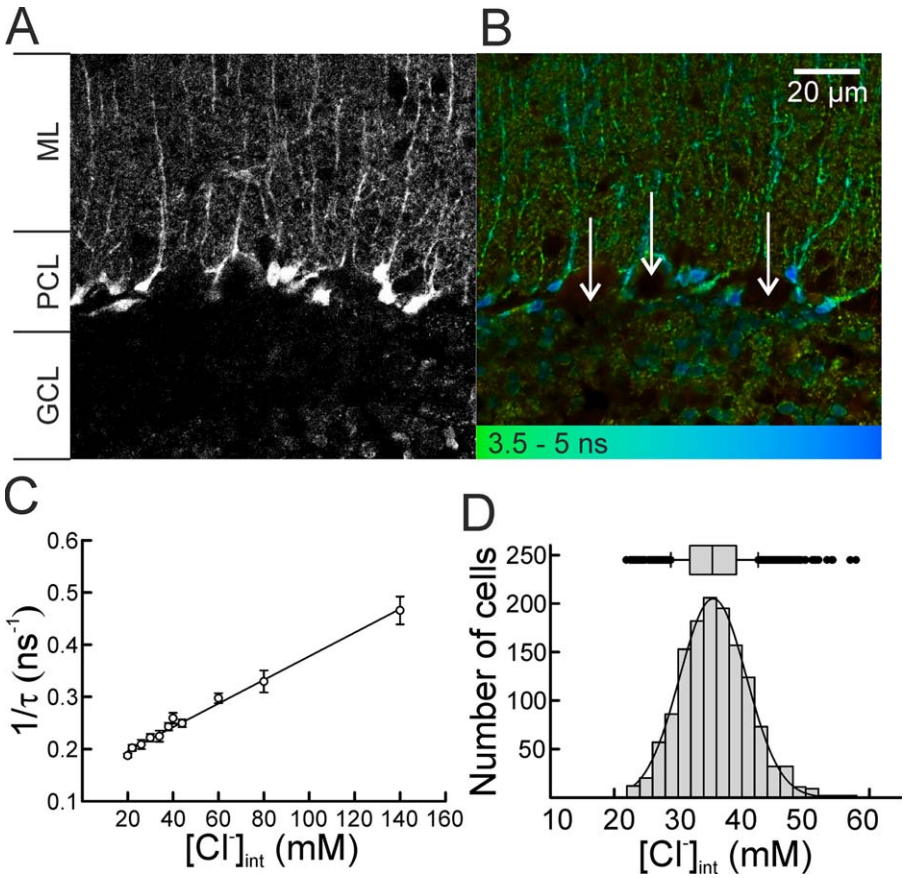

FIGURE 1: FLIM of intracellular chloride concentrations in Bergmann glial cells. (A,B) Representative fluorescence intensity (GFP ex: 910 nm) (A) and fluorescence lifetime (MQAE ex: 750 nm, em: SP500) (B) image of a GFAP-GFP WT acute cerebellar slice loaded with MQAE. Average fluorescence lifetimes in (B) are color coded, Purkinje neurons are indicated by arrows. (C) Chloride dependence of the MQAE fluorescence lifetime in Bergmann glia. Data points represent the inverse average fluorescence lifetime measured for different chloride concentrations (20 −140 mM, $n>8$ cells). Error bars indicate 95% CI and the solid line represents a linear fit ($R^2= 0.92$) with $K_{SV}= 14.97\ M^{-1}$. (D) Distribution of $[Cl^-]_{int}$ of all measured Bergmann glial cells pooled from all ages older than P20. The solid line represents a Gaussian fit with a mean ± SD of 35.3 ± 6.3 mM (1,355 cells, 84 slices, 33 animals).

relationship between fluorescence lifetime and chloride concentration (Verkman, 1990):

$$\frac{\tau_0}{\tau} = 1 + K_{SV}[Cl^-]_{int}$$

where τ is the MQAE fluorescence lifetime at this $[Cl^-]_{int}$, τ_0 is the MQAE fluorescence lifetime in the absence of chloride, and K_{SV} is the cell-specific Stern–Volmer constant.

We measured the fluorescence intensity and lifetime in FLIM images of acute sagittal cerebellar slices (Bennay et al., 2008) loaded with MQAE using two-photon excitation (Kaneko et al., 2004; Fig. 1). Both images show the characteristic three-layer structure of the cerebellar cortex: the inner granule cell layer, containing granule cells together with inhibitory interneurons and astrocytes; the Purkinje cell layer, harboring Purkinje cell and Bergmann glial cell somata; and the external molecular layer, containing the dendritic trees of Purkinje neurons, parallel fibers originating from granule cells, and the radial branches of Bergmann glial cells (Fig. 1A, B). Bergmann glial cells are easily identified by their unipolar morphology, size, and location in the Purkinje cell layer around the Purkinje neurons (Fig. 1A). Since Bergmann glial cells accumulate much more MQAE compared with Purkinje neurons, Bergmann glial cells and Purkinje neurons are additionally distinguished by differences in fluorescence intensity in MQAE-loaded cerebellar slices. This assignment of Bergmann glial cells was verified in transgenic mice expressing EGFP controlled by a GFAP promoter (Zhuo et al., 1997) (Fig. 1A).

Fluorescence lifetimes in Bergmann glial somata have significantly longer fluorescence lifetimes compared with the surrounding cells (Fig. 1B). However, cell-specific differences in Stern–Volmer constants mean that fluorescence lifetimes cannot be directly compared between different cell types. To determine K_{SV} values in Bergmann glial cells, $[Cl^-]_{int}$ was adjusted by changing extracellular chloride concentrations in the presence of two ionophores, nigericin and tributyltin, and an extracellular $[K^+]$ of 140 mM (Bevensee et al., 1997; Chao et al., 1989; Gensch et al., 2015; Kaneko et al., 2004).

Linear regression analysis of the inverse of the average fluorescence lifetimes at different chloride concentrations provided the K_{SV} for MQAE in Bergmann glial cells (14.97 M^{-1}; Fig. 1C). Using this value, an average $[Cl^-]_{int}$ of 35.3 ± 0.3 mM was determined from 1355 Bergmann glial cell somata in 84 cerebellar slices from 33 mice (at P20–P100; Fig. 1D). The glial $[Cl^-]_{int}$ is thus well above the calculated diffusion equilibrium (around 6 mM), indicating that adult Bergmann glial cells actively accumulate chloride.

NKCC1 Accumulates Chloride in Bergmann Glial Cells

Bergmann glial cells express three types of electroneutral cation–chloride cotransporters of the solute carrier 12 (SLC12) family: NKCC1, KCC1, and KCC3 (Mount et al., 1999; Yan et al., 2001). NKCC1 accumulates Cl^- by coupling its movement to the inward directed transmembrane Na^+ gradient; it might thus be responsible for increasing the glial $[Cl^-]_{int}$ to above equilibrium. In contrast, KCC1 and KCC3 mediate chloride–potassium efflux and might reduce $[Cl^-]_{int}$ to below the equilibrium values for NKCC1 transporters.

To investigate whether these cotransporters affect chloride accumulation, we incubated acute cerebellar slices with either bumetanide (40 μM, 10 min), which specifically blocks NKCC1 (Payne et al., 2003), or DIOA (80 μM, 20 min), which blocks KCC 1–3 with comparable efficiency (Mercado et al., 2000), prior to FLIM (Fig. 2). Whereas bumetanide decreased $[Cl^-]_{int}$ to 30.0 ± 0.8 mM (221 cells, nine slices, three animals), we did not observe any significant differences in $[Cl^-]_{int}$ between cerebellar slices incubated in DIOA (34.1 ± 0.9 mM; 114 cells, five slices, three animals) and untreated controls. These results demonstrate that NKCC1 induces chloride accumulation in Bergmann glia, whereas neither KCC1 nor KCC3 regulate $[Cl^-]_{int}$ under physiological conditions.

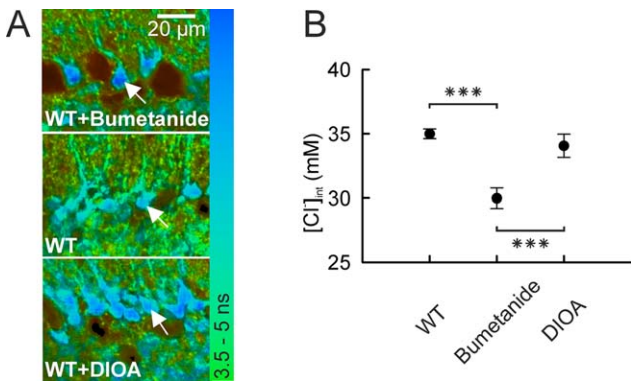

FIGURE 2: NKCC1 accumulates chloride in Bergmann glial cells. (A) Representative FLIM image of WT acute cerebellar slices under control conditions (Ctrl, middle image) or incubated with Bumetanide (upper image) or DIOA (lower image, representative Bergmann glial cells are indicated by arrows). Average fluorescence lifetimes are color coded. (B) The $[Cl^-]_{int}$ of WT Bergmann glial cells after incubation with 40 μM bumetanide (221 cells, nine slices, three animals) or 80 μM DIOA (114 cells, five slices, three animals). Data are means ± 95% confidence intervals.

Anion Channels Associated with Glutamate Transporters Modify $[Cl^-]_{int}$ in Bergmann Glia

Adult cerebellar Bergmann glial cells have a stable negative resting potential that is generated by a predominant resting potassium conductance (Bergles et al., 1997). Three types of chloride channels might use this electrical gradient to counteract active chloride accumulation by passive chloride efflux: volume-activated anion channels (VRAC/VSOC; Kimelberg et al., 2006; Mongin, 2015); the voltage-gated chloride channel ClC-2 (Hoegg-Beiler et al., 2014; Kimelberg et al., 2006; Makara et al., 2003); or anion channels associated with glial EAATs (Fahlke et al., 2016; Fairman et al., 1995; Machtens et al., 2015; Wadiche et al., 1995). Since astrocytic volume-activated anion channels are mainly closed under physiological conditions (Mongin, 2015), we decided to focus on the ClC-2 and EAAT anion channels.

ClC-2 exhibits voltage- and anion-dependent gating, which appears to be uniquely suited to reducing $[Cl^-]_{int}$ (Kimelberg et al., 2006; Stölting et al., 2014). Moreover, earlier work demonstrated that gene transfer of the ClC-2 chloride channel into cultured dorsal root ganglion neurons resulted in a pronounced reduction of $[Cl^-]_{int}$ and shift of the chloride equilibrium potential to more negative values (Staley et al., 1996). Since no effective ClC-2 blockers are available (Zifarelli and Pusch, 2012), we used homozygous knockout animals (Nehrke et al., 2002) to investigate whether ClC-2 regulates $[Cl^-]_{int}$ in Bergmann glial cells. Adult *Clcn2*$^{-/-}$ mice suffer from leukoencephalopathy with white matter spongiform vacuolation (Blanz et al., 2007), and we therefore studied Bergmann glial cells from juvenile (P20) *Clcn2*$^{-/-}$ mice. Chloride concentrations in these animals (34.3 ± 1.3 mM; 148 cells, 10 slices, three animals) were indistinguishable from those of juvenile WT animals (Fig. 3A). We conclude that ClC-2 does not contribute to $[Cl^-]_{int}$ regulation in Bergmann glial cells under our experimental conditions.

EAATs are the main glutamate uptake carriers in the mammalian central nervous system and also function as ligand-gated anion channels (Fahlke et al., 2016; Fairman et al., 1995; Machtens et al., 2015; Wadiche et al., 1995). Bergmann glial cells express two members of this family: EAAT1 (or GLAST; encoded by *Slc1a3*) and EAAT2 (or GLT-1; encoded by *Slc1a2*; Lehre et al., 1995; Torp et al., 1994). Since larger anion currents are associated with EAAT1/GLAST than with EAAT2/GLT-1, we initially studied the role of EAAT1/GLAST on chloride concentrations in Bergmann glial cells using *Slc1a3*$^{-/-}$ knock-out animals

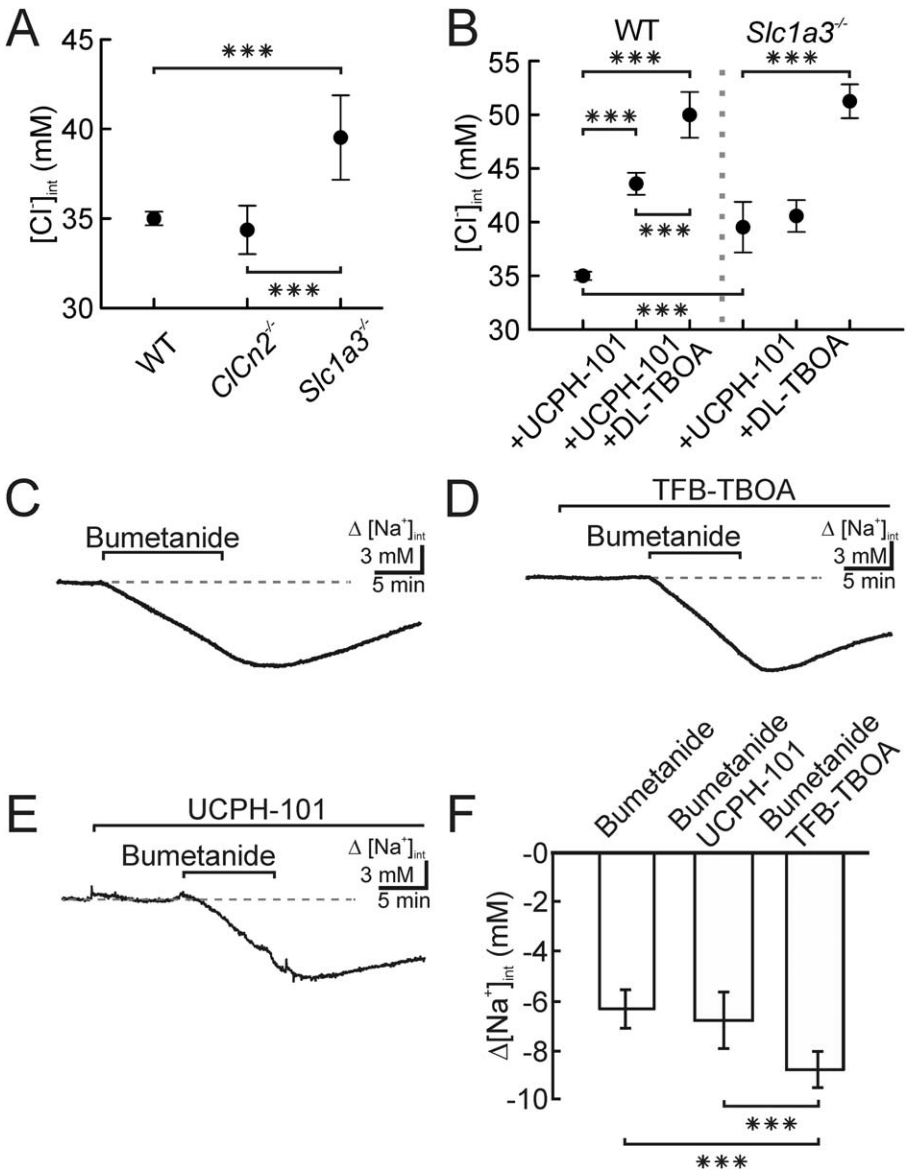

FIGURE 3: EAAT1/GLAST and EAAT2/GLT-1 regulate $[Cl^-]_{int}$ in Bergmann glial cells. (A) Intracellular chloride concentration of Bergmann glial cells from WT, *Clcn2*$^{-/-}$, and *Slc1a3*$^{-/-}$ mice. (B) Changes in $[Cl^-]_{int}$ in WT or *Slc1a3*$^{-/-}$ Bergmann glial cells after incubation with 10 μM UCPH-101 and/or 100 μM DL-TBOA. (C–E) Averaged $[Na^+]_{int}$ responses to treatment with 40 μM bumetanide (C) and either 1 μM TFB-TBOA (D) or 10 μM UCPH-101 (E). Traces represent averages obtained from 36 cells (bumetanide), 64 cells (TFB-TBOA), and 36 cells (UCPH-101). (F) Histogram summarizing the changes in $[Na^+]_{int}$ as determined after 10 min of incubation with the different drugs. Data are means ± 95% confidence intervals.

(Watase et al., 1998) or specific pharmacological block. The $[Cl^-]_{int}$ of Bergmann glial cells was significantly higher in juvenile (P20) *Slc1a3*$^{-/-}$ mice than in WT animals (39.5 ± 2.3 mM; 182 cells, 18 slices, eight animals; Fig. 3A). Further, the EAAT1/GLAST-specific high-affinity blocker UCPH-101 (Abrahamsen et al., 2013; Jensen et al., 2015) increased $[Cl^-]_{int}$ to 43.6 ± 1.0 mM (418 cells, 40 slices, 17 animals) in WT, but had no obvious effect on *Slc1a3*$^{-/-}$ Bergmann glial cells (Fig. 3B). To test whether EAAT2/GLT-1 also contributes to glial chloride homeostasis, we incubated *Slc1a3*$^{-/-}$ cerebellar slices in 100 μM DL-TBOA, a glutamate uptake blocker with a higher affinity for EAAT2/GLT-1 than for EAAT1/GLAST (Jensen et al., 2015). Under these conditions, $[Cl^-]_{int}$ in *Slc1a3*$^{-/-}$ Bergmann glial cells (51.2 ± 1.6 mM; 93 cells, 13 slices, three animals) was similar to that of WT in which EAAT1/GLAST and EAAT2/GLT-1 were simultaneously blocked by UCPH-101 and DL-TBOA (50.0 ± 2.1 mM; 63 cells, seven slices, two animals, Fig. 3B). This result indicates that the observed differences in $[Cl^-]_{int}$ of WT and *Slc1a3*$^{-/-}$ Bergmann glial cells is not due to the up- or downregulation of other anion transport proteins in knock-out animals.

UCPH-101 and DL-TBOA likely modify the $[Cl^-]_{int}$ by preventing EAAT anion channel opening (21). Alternatively, blocking glutamate transport might cause glutamate excitotoxicity, increase the extracellular $[Na^+]$ and $[K^+]$, and thus indirectly increase $[Cl^-]_{int}$ by stimulating glial chloride uptake via NKCC1 (Su et al., 2002). We therefore quantified the effects of UCPH-101 and DL-TBOA on NKCC1 activity by studying the effects of Bumetanide (40 µM, 10 min) on the intracellular sodium concentration of Bergmann glial cells ($[Na^+]_{int}$; Fig. 3C–F). Both EAAT blockers did not influence the baseline $[Na^+]_{int}$ (Fig. 3D,E), supporting earlier results that glutamate transport inhibitors do not affect astrocytic sodium concentration (Karus et al., 2015). Treatment with bumetanide alone decreased $[Na^+]_{int}$ by 6.3 ± 0.4 mM (36 cells, four slices, three animals; Fig. 3C). This bumetanide-mediated decrease in $[Na^+]_{int}$ was unaffected by 10 µM UCPH-101 (6.8 ± 0.6 mM; 64 cells, five slices, three animals, Fig. 3E), indicating that EAAT1/GLAST inhibition did not result in a secondary, additional activation of NKCC1 and increased import of chloride through this transporter. With combined inhibition of EAAT1/GLAST and EAAT2/GLT-1 by TFB-TBOA (1 µM) (Shimamoto et al., 2004), $[Na^+]_{int}$ dropped by 8.8 ± 0.4 mM (36 cells, three slices, two animals, Fig. 3D), which was slightly, but significantly higher than that obtained with bumetanide alone (Fig. 3C,D and F). This difference might be due to TFB-TBOA-mediated increases in neuronal $[Na^+]$ (Karus et al., 2015; Langer and Rose, 2009) causing loss of neuronal K^+ and additional activation of NKCC1 in Bergmann glia. Based on these data, we conclude that pharmacological blockade of EAAT glutamate transporters do not modify glial $[Cl^-]_{int}$ via altering NKCC1 activity.

Age-Dependent Regulation of the Intraglial [Cl⁻]

Whereas developmental changes in neuronal $[Cl^-]_{int}$ have been studied in great detail (Rivera et al., 1999), it is unclear whether glial cells also modify $[Cl^-]_{int}$ during maturation. Fig. 4 shows representative FLIM images of MQAE-loaded acute cerebellar slices from mice at P5, P8, and P13. Between E15 and P7, the precursors of Bergmann glial cells and Purkinje neurons migrate from the ventricular neuroepithelium toward the prospective cerebellar cortex (Yamada and Watanabe, 2002). At P5, these two layers are still visible (Fig. 4A, P5), but at the end of the first postnatal week Purkinje neurons and Bergmann glial cells have aligned to form a monolayer (Fig. 4A, P8 and P13).

We found that MQAE fluorescence lifetimes were significantly smaller at P5–P6 than at P20. To test whether age-dependent differences in K_{SV} in the Bergmann glial cells contribute to these differences we measured fluorescence lifetimes at pre-determined $[Cl^-]_{int}$ during calibration experiments. The thus obtained lifetimes were the same as in older animals (Supp. Info. Fig. S1), demonstrating that difference in fluorescence lifetimes is due to developmental changes in glial chloride concentrations. Fig. 4B shows age-dependent changes in $[Cl^-]_{int}$ between P5 and P100. In cerebellar Bergmann glial cells from WT animals, chloride concentrations are very high at P5, decrease to adult levels at P13, and remain stable until P100 (Fig. 4B). The $[Cl^-]_{int}$ in *Slc1a3*$^{-/-}$

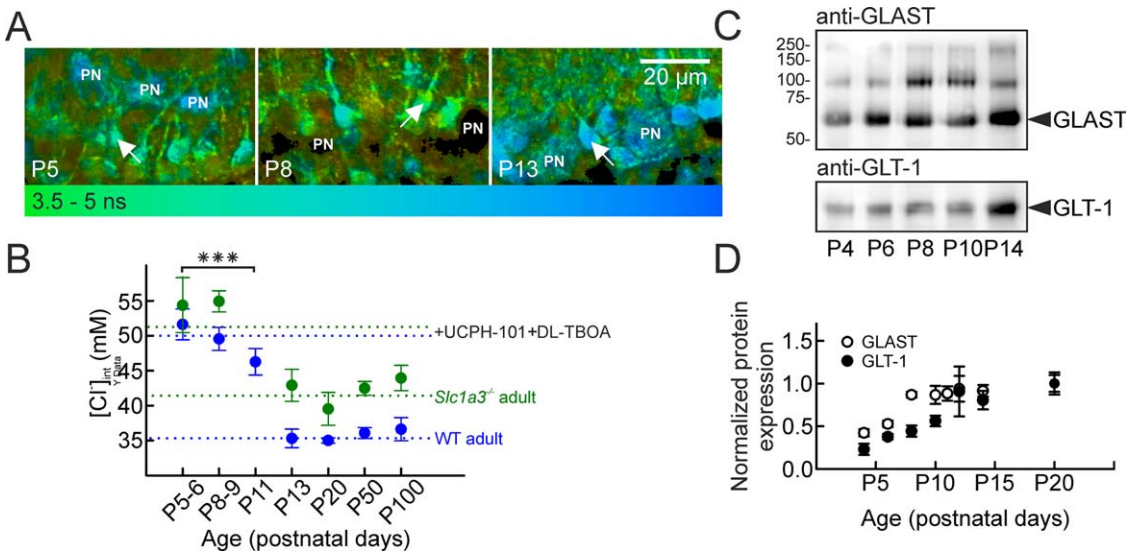

FIGURE 4: Age-dependent changes of $[Cl^-]_{int}$ in Bergmann glial cells. (A) Representative FLIM images of WT acute cerebellar slices from young animals at P5–P13. PN, Purkinje neuron, the arrows point to Bergmann glial cells. (B) Age dependence of $[Cl^-]_{int}$ in Bergmann glial cells from WT or *Slc1a3*$^{-/-}$ animals. All data are means ± 95% confidence intervals. (C) Western blots showing EAAT1/GLAST and EAAT2/GLT-1 expression in WT animals at different postnatal ages. (D) Age dependence of EAAT1/GLAST and EAAT2/GLT-1 expression levels normalized to total loaded protein. Data are means ± SEM.

animals exhibit a similar age dependency but are always larger than the corresponding WT values.

Earlier studies reported that EAAT1/GLAST is expressed from P5 onward and gradually increases until P20 in Bergmann glial cells, whereas EAAT2/GLT-1 expression is negligible until P14 and then increases more steeply with age (Holmseth et al., 2012; Lehre and Danbolt, 1998; Regan et al., 2007). We determined EAAT1/GLAST and EAAT2/GLT-1 expression in WT and *Slc1a3*$^{-/-}$cerebellums at different ages and observed changes in expression (Fig. 4C,D) that can account for the distinct developmental $[Cl^-]_{int}$ patterns in WT and *Slc1a3*$^{-/-}$ animals (Fig. 4B).

EAAT Anion Conduction Permits Dynamic Modification of Glial $[Cl^-]_{int}$

Since the open probability of EAAT anion channels depends on the synaptic glutamate concentration (Bergles et al., 1997; Machtens et al., 2015), we reasoned that activation of EAAT1/GLAST and/or EAAT2/GLT-1 anion channels by synaptically released glutamate might enhance chloride efflux and decrease the $[Cl^-]_{int}$. Cerebellar Purkinje neurons receive excitatory input by both climbing and parallel fibers, and activation of these synapses evokes glutamate transporter currents in Bergmann glial cells (Bergles et al., 1997). To study the effects of cerebellar activity on glial $[Cl^-]_{int}$, we stimulated parallel fibers via a bipolar electrode positioned within the molecular cell layer with a pulse protocol resembling physiological parallel fiber activity (series of 20 pulses of 10 mA (150 μs duration) at 200 Hz; pulse series repeated at a frequency of 0.1 Hz for 1 min; van Beugen et al., 2013). $[Cl^-]_{int}$ was measured twice before and twice after each pulse series (indicated by a gray line in Fig. 5A). Each individual measurement lasted about 80 s, and we were therefore unable to perform such experiments at higher temporal resolution.

In WT cells, electrical stimulation of the glutamatergic afferents reduced the $[Cl^-]_{int}$ from 34.1 ± 2.0 to 26.9 ± 1.7 mM (24 cells, six slices, four animals; Fig. 5A,B). We observed similar activity-induced $[Cl^-]_{int}$ changes in cerebellar slices perfused with 50 μM bicuculline, a specific blocker of ionotropic GABA receptors (Curtis et al., 1970), and in control slices (Fig. 5B). The decrease in $[Cl^-]_{int}$ upon stimulation was therefore not due to $GABA_A$ receptor opening, in full agreement with the notion that synaptically released glutamate modifies intracellular anion concentrations by increasing EAAT anion channel conductance. Activation of the parallel fibers in *Slc1a3*$^{-/-}$ had less pronounced effects on $[Cl^-]_{int}$ in Bergmann glial cells, in agreement with the smaller contribution of EAAT2/GLT-1 anion channels to glial anion concentrations (Fig. 5C). Experiments on *Clcn2*$^{-/-}$ cerebellar slices revealed similar dynamic alterations in $[Cl^-]_{int}$ as those seen in WT animals (Fig. 5C).

Discussion

We here used FLIM in acute cerebellar slices obtained from neonate, juvenile and adult animals to measure the $[Cl^-]_{int}$ in Bergmann glial cells and investigate their regulation by chloride channels and transporters. We determined the resting $[Cl^-]_{int}$ of adult Bergmann glial cells to be 35.3 ± 0.3 mM and identified two main determinants of this parameter: the Na^+–K^+−$2Cl^-$ cotransporter NKCC1 and the glutamate transporters EAAT1/GLAST and EAAT2/GLT-1. Glial $[Cl^-]_{int}$ is in a dynamic equilibrium between secondary-active Cl^- inward transport and passive efflux through EAAT anion channels. Its value therefore does not only depend on the driving forces of these two transport proteins, but also on their numbers and activities. This mechanism permits adjustment of $[Cl^-]_{int}$ by regulatory pathways modifying the transport activity of NKCC1 or the open probability of EAAT anion channels, even without changes in their driving force.

At first glance, a role in modifying intracellular ion concentrations seems surprising for chloride channels. Channel-mediated ion fluxes often modify the cellular membrane potential and thus prevent long-lasting ion influx or efflux necessary for significant changes in ion concentrations. However, in adult Bergmann glial

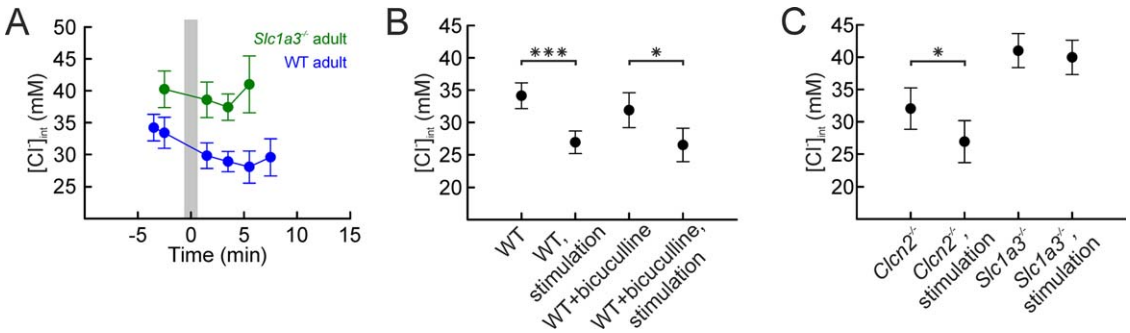

FIGURE 5: Dynamic changes in Bergmann glial $[Cl^-]_{int}$ during cerebellar excitation. (A) Averaged $[Cl^-]_{int}$ responses of WT and *Slc1a3*$^{-/-}$ Bergmann glial cells to electrical stimulation (indicated by a gray box). (B) $[Cl^-]_{int}$ of WT Bergmann glial cells before and after electrical stimulation in the absence or presence of 50 μM bicuculline. (C) $[Cl^-]_{int}$ in *Slc1a3*$^{-/-}$or *Clcn2*$^{-/-}$ Bergmann glial cells before and after electrical stimulation. All data are means ± 95% confidence intervals.

cells the resting membrane potential is clamped to the K^+ equilibrium potential by a large potassium conductance (Bergles and Jahr, 1997; Bordey and Sontheimer, 1997). Under these conditions chloride effluxes through EAAT anion channels will not significantly depolarize Bergmann glial cells, so that continuous chloride currents and establishment of a new equilibrium $[Cl^-]_{int}$ are possible. At early developmental stages the glial potassium conductance is not as dominant, and the chloride conductance might contribute to the resting potential at such stages. However, because of Cl^- accumulation by NKCC1 the resting potential will be always more negative than the Cl^- reversal potential, permitting Cl^- efflux through EAAT anion channels.

Blocking NKCC1 decreased the $[Cl^-]_{int}$ in Bergmann glial cells, although not to the values expected for passive distribution (Fig. 2). Moreover, even though NKCC1 transports Na^+ and Cl^- in a stoichiometry of 1:2 (Haas and Forbush, 2000), bumetanide reduced $[Na^+]_{int}$ and $[Cl^-]_{int}$ by similar amounts (Figs. 2 and 3). These two results suggest that NKCC1 together with additional - yet to be defined - transporters accumulate chloride in Bergmann glial cells. Changes in EAAT glutamate transporter expression or activity modified the Bergmann glial $[Cl^-]_{int}$ (Figs. 3–5). EAATs mediate secondary active glutamate transporters and also function as anion-selective channels (Fahlke et al., 2016; Fairman et al., 1995; Machtens et al., 2015; Wadiche et al., 1995). Although these two transport functions are not separable by either pharmacological or genetic tools (Jensen et al., 2015), our results on astrocytic $[Cl^-]_{int}$ can all be convincingly explained by assuming that blocking or activating EAATs change glial $[Cl^-]_{int}$ via altering the EAAT chloride conductance. We experimentally excluded two alternative explanations. The $GABA_A$-specific blocker bicuculline did not modify the response of glial $[Cl^-]_{int}$ to synaptic activity (Fig. 5) or to EAAT1/GLAST blockade with UCPH-101 (Supp. Info. Fig. S2). This result demonstrates that blocking EAATs does not modify $[Cl^-]_{int}$ by impaired synaptic inhibition and decreased chloride efflux through ionotropic GABA receptors. Moreover, we demonstrated that blocking EAAT1/GLAST, the predominant glutamate uptake mechanism in Bergmann glial cells, does not enhance NKCC1 activity (Fig. 3), indicating that reduced glutamate transporter activity does not affect glial $[Cl^-]_{int}$ via increased external $[Na^+]$ and $[K^+]$ due to glutamate excitotoxicity. Combined inhibition of both EAAT1/GLAST and EAAT2/GLT-1 revealed a slight additional stimulation of NKCC1 under this condition, which might result in slightly larger $[Cl^-]_{int}$ than caused by inhibition of chloride efflux through EAAT anion channels alone. All other consequences of increased glutamate concentration are not expected to modify glial chloride concentrations. We thus conclude that EAAT anion channels regulate intracellular chloride concentrations in Bergmann glial cells.

We tested further chloride channels and transporters that have been shown to play a role in intracellular chloride regulation in other cell types, ClC-2 (Staley et al., 1996) and KCC1 and KCC3 (Boettger et al., 2003; Gagnon et al., 2007; Gagnon and Delpire, 2013). Whole-cell recordings revealed large ClC-2 currents in Bergmann glial cells (Hoegg-Beiler et al., 2014), indicating expression and activity of these channels in this type of cells. However, genetic ablation of *Clcn2* neither modifies resting Bergmann glial $[Cl^-]_{int}$ (Fig. 3) nor dynamic changes upon electrical stimulation (Fig. 5). KCC1 or KCC3 mediate coupled K^+-Cl^- transport in Bergmann glia (Kanaka et al., 2001; Shekarabi et al., 2011), but pharmacological block leaves $[Cl^-]_{int}$ unaffected (Fig. 2). These findings indicate that neither ClC-2 nor KCC1 and KCC3 contribute to the resting $[Cl^-]_{int}$ in these cells. Our results thus demonstrate a unique role of EAAT anion channels in intracellular chloride regulation in Bergmann glial cells.

Anion concentrations and glutamate transporter levels display opposite age dependencies (Fig. 4). A drop in Bergmann glial intracellular chloride concentrations from >50 mM to the adult value of 35 mM is coincident with the age-related upregulation of EAAT1/GLAST and EAAT2/GLT-1 (Fig. 4; Regan et al., 2007) and the development of parallel fiber to Purkinje cell synapses (Yamada, 2000). Combined blockade of EAAT1/GLAST and EAAT2/GLT-1 in cerebellar slices from adult animals restored Bergmann glial cell chloride concentrations to the high levels seen at P5–P6 (Figs. 3 and 4). *Slc1a3*$^{-/-}$ glial cells have higher $[Cl^-]_{int}$ compared with WT cells at all developmental stages tested, although the differences are smaller in young than in adult animals. This is fully consistent with the temporal similarities in expression for EAAT1/GLAST and EAAT2/GLT-1: early postnatal onset and upregulation until P14 (Fig. 4). Taken together, these results indicate that changes in EAAT1/GLAST and EAAT2/GLT-1 expression levels and activity are responsible for the developmental glial chloride switch.

Bergmann glial cells are generated in the ventricular zone as radial glial cells that start migrating radially toward the cortex at around E15 (Yuasa, 1996). It is tempting to speculate that high glial $[Cl^-]_{int}$ supports glial migration during cerebellar ontogeny by allowing the necessary rapid volume adjustments (Habela et al., 2009; Kahle et al., 2010). At P15, when glial $[Cl^-]_{int}$ adopts the adult values, these migratory processes are all completed (Komuro et al., 2001). The importance of high $[Cl^-]_{int}$ for cell migration and division and the importance of EAAT glutamate transporters in regulating $[Cl^-]_{int}$ is illustrated by malignant glioma cells that quickly reproduce and infiltrate into surrounding brain (Habela et al., 2009). These cells lack EAAT glutamate

transporters and exhibit high intracellular anion concentrations (~100 mM; Robert and Sontheimer, 2014).

Astrocytic GABA transporters (GAT1, GAT3) mediate GABA reuptake from the extracellular medium (Zhou and Danbolt, 2013) by coupling the movement of one GABA molecule to the symport of two Na^+ ions and one Cl^- ion (Zomot et al., 2007). GATs are known to work close to equilibrium and switch from GABA uptake to release in response to changes in the driving force (Barakat and Bordey, 2002; Richerson and Wu, 2003). External [GABA] ($[GABA]_{ext}$) in the perisynaptic space is therefore expected to be close to values at which GATs are at equilibrium level:

$$[GABA]_{ext} = \frac{[Na^+]_{int}^2 [Cl^-]_{int} [GABA]_{int}}{[Na^+]_{ext}^2 [Cl^-]_{ext}} e^{\frac{UF}{RT}}$$

By assuming standard $[Na^+]_{ext}$ and $[Cl^-]_{ext}$, an internal [GABA] of 2.3 mM (Lee et al., 2011; Zomot et al., 2007), and an internal $[Na^+]$ of 14.6 mM (Rose and Ransom, 1996), we calculated an equilibrium external [GABA] of about 0.2 μM for adult WT animals. The high $[Cl^-]_{int}$ of 52 mM in very young animals (P5) predicted an external [GABA] above 0.35 μM, assuming age-independent $[Na^+]_{int}$. EAAT-mediated changes of $[Cl^-]_{int}$ might thus contribute to adjusting external [GABA].

Such changes in $[GABA]_{ext}$ potentially modify cerebral development and the function of the adult cerebellum. In the cerebellar cortex, granule cells and Purkinje neurons express high affinity $GABA_A$ receptors (Saxena and Macdonald, 1996) that conduct tonic GABAergic currents due to high resting open probabilities (Brickley et al., 1996). These receptors modulate migration of immature neurons (Luhmann et al., 2015), and the glial chloride switch might thus contribute to the termination of neuronal migration at P15 via altering resting $[GABA]_{ext}$ (Fig. 4). Since the glial chloride switch occurs at the same time as the neuronal chloride switch, it might further facilitate inhibitory synaptic transmission. In the adult cerebellum EAAT-mediated changes in Bergmann glial $[Cl^-]_{int}$ (Fig. 5) might partially compensate for changes in $[Na^+]_{int}$ upon parallel fiber activation (Bennay et al., 2008; Kirischuk et al., 2007) and prevent significant changes in external equilibrium [GABA] concentration during cerebellar activity. During brain ischemia or neuronal death, increased levels of external glutamate would activate EAATs and probably decrease glial $[Cl^-]_{int}$ to values significantly below those reached in our stimulation experiments. Intracellular $[Na^+]$ is also expected to rise, and changes in chloride concentrations might restrict elevation of $[GABA]_{ext}$. Naturally occurring *SLC1A3* gain-of-function mutations - which have been identified in patients with episodic ataxia and epilepsy (Winter et al., 2012) - may reduce glial chloride concentrations, stimulate GABA uptake and reduce synaptic inhibitionin ataxia and epilepsy.

Bergmann glial cells exhibit a complex architecture with cell soma, several radial fibers and multiple short simple thorns and longer complex appendages branching from the radial fibers (Grosche et al., 1999). The appendages represent up to 90% of the total surface area and might thus be of major importance for salt and solute transport in this class of cells. Moreover, glutamatergic synapses are surrounded by glial sheaths (Grosche et al., 2002). Synaptic release of glutamate into these microdomains (Grosche et al., 1999) will therefore lead to higher glutamate concentrations closer to the appendages than around the soma. Since EAAT1 and EAAT2 are uniformly distributed in Bergmann glial cells (Lehre and Danbolt, 1998), EAAT-mediated chloride fluxes per volume unit are expected at comparable glutamate concentrations to be more pronounced in glial appendages than in the soma. Under resting conditions, $[Cl^-]_{int}$ in the appendages might therefore be lower than in the soma, and activity-mediated changes in $[Cl^-]_{int}$ might be more pronounced. Unfortunately, it is not possible to measure $[Cl^-]_{int}$ in these extensions using our current approach. Due to the small dimensions we are unable to distinguish fluorescence lifetimes in such glial extensions from neighboring neurons, preventing accurate lifetime measurements and calibration. This restriction might be overcome by directly loading individual Bergmann glial cells via patch pipettes, however, this modification is out of scope of our present work.

Our conclusion that EAAT anion channels modify $[Cl^-]_{int}$ in Bergmann glial cells is based on the variation of this parameter upon blocking or removing these proteins. Under certain conditions such differences were only small. For example, $[Cl^-]_{int}$ in *Slc1a3*$^{-/-}$ Bergmann glial cells differed from WT only by 4.5 mM. The broad dynamic range of MQAE fluorescence lifetimes and the high precision of time correlated single photon counting (TCSPC) experiments makes the combination of both techniques very sensitive and accurate and certainly suited to measure such small differences in $[Cl^-]_{int}$. The precision of fluorescence lifetime determination by TCSPC depends on the number of detected photons, the observation time window, and the fluorescence lifetime value (Maus et al., 2001; Becker, 2005; Becker, 2015). Under our experimental conditions, the expected relative error of fluorescence lifetimes in Bergmann glia is less than 1.35%, and for cells with average number of detected photons or more even below 0.55%. These estimates indicate that we can indeed distinguish Bergmann glial cells even with the smallest observed difference in $[Cl^-]_{int}$, 4.38 ± 0.015 ns/35.0 ± 0.3 mM in WT vs. 4.18 ± 0.034 ns/39.5 ± 2.4 mM in *Slc1a3*$^{-/-}$ mice. The large number of experimental repetitions results in very narrow, non-overlapping 95% confidence

intervals (Fig. 3A). In cells intracellularly dialyzed with $[Cl^-]_{int}$ of 34 mM in the presence of nigericin and tributyltin, we obtained significantly different fluorescence lifetimes compared to cells at 38 mM (Supp. Info. Table 1).

EAATs are prototypic dual function proteins that are secondary-active glutamate transporters and anion channels. For many years, the molecular basis of EAAT anion conduction was not understood, raising doubts whether anions permeate through defined anion-selective ion conduction pathways or just slip through defective states in imperfectly working transporters. Work in recent years clarified this particular function of EAAT glutamate transporters (Fahlke et al., 2016). EAAT anion channels are now known to exhibit unitary conductances in the range of other anion channels and to be perfectly selective for anions. Machtens et al. (2015) demonstrated that anions permeate through an aqueous conduction pathway at the interface between the trimerization and the transport domain that opens and closes upon the lateral movement of the transport domain from intermediate transport conformations.

We now report that developmental upregulation or activation of EAAT1/GLAST and EAAT2/GLT-1 anion channels by increased perisynaptic glutamate levels reduce glial chloride concentrations. Such changes in glial $[Cl^-]_{int}$ permit a crosstalk of glutamatergic synaptic transmission with multiple other signaling pathways in the mammalian central nervous system. This function highlights the importance of coupling anion channels and glutamate carriers in EAAT glutamate transporters and predicts additional important roles of these dual function proteins in normal and pathological brain function.

Acknowledgment

Grant sponsor: Deutsche Forschungsgemeinschaft Grant SPP 1757; Grant number: Ro2327/8-1

The authors thank Drs. Niels C. Danbolt, Raul Guzman, Patricia Hidalgo, Karl W. Kafitz, Daniel Kortzak, Jan-Philipp Machtens, Frank Müller, Ingo Weyand, and Gabriel Stölting for helpful discussions and Christoph Aretzweiler for technical assistance.

References

Abrahamsen B, Schneider N, Erichsen MN, Huynh TH, Fahlke Ch, Bunch L, Jensen AA. 2013. Allosteric modulation of an excitatory amino acid transporter: The subtype-selective inhibitor UCPH-101 exerts sustained inhibition of EAAT1 through an intramonomeric site in the trimerization domain. J Neurosci 33:1068–1087.

Barakat L, Bordey A. 2002. GAT-1 and reversible GABA transport in Bergmann glia in slices. J Neurophysiol 88:1407–1419.

Becker 2005. Advanced time-correlated single photon counting techniques. Springer Series in Chemical Physics 81: (doi: 10.1007/3-540-28882-1).

Becker 2015. Advanced Time-Correlated Single Photon Counting Applications. Springer Series in Chemical Physics 111: (doi: 10.1007/978-3-319-14929-5).

Bekar LK, Walz W. 2002. Intracellular chloride modulates A-type potassium currents in astrocytes. Glia 39:207–216.

Bennay M, Langer J, Meier SD, Kafitz KW, Rose CR. 2008. Sodium signals in cerebellar Purkinje neurons and Bergmann glial cells evoked by glutamatergic synaptic transmission. Glia 56:1138–1149.

Bergles DE, Dzubay JA, Jahr CE. 1997. Glutamate transporter currents in bergmann glial cells follow the time course of extrasynaptic glutamate. Proc Natl Acad Sci USA 94:14821–14825.

Bergles DE, Jahr CE. 1997. Synaptic activation of glutamate transporters in hippocampal astrocytes. Neuron 19:1297–1308.

Bevensee MO, Apkon M, Boron WF. 1997. Intracellular pH regulation in cultured astrocytes from rat hippocampus. II. Electrogenic Na/HCO_3 cotransport. J Gen Physiol 110:467–483.

Blanz J, Schweizer M, Auberson M, Maier H, Muenscher A, Hubner CA, Jentsch TJ. 2007. Leukoencephalopathy upon disruption of the chloride channel ClC-2. J Neurosci 27:6581–6589.

Boettger T, Rust MB, Maier H, Seidenbecher T, Schweizer M, Keating DJ, Faulhaber J, Ehmke H, Pfeffer C, Scheel O, et al. 2003. Loss of K-Cl co-transporter KCC3 causes deafness, neurodegeneration and reduced seizure threshold. EMBO J 22:5422–5434.

Bordey A, Sontheimer H. 1997. Postnatal development of ionic currents in rat hippocampal astrocytes in situ. J Neurophysiol 78:461–477.

Brickley SG, Cull-Candy SG, Farrant M. 1996. Development of a tonic form of synaptic inhibition in rat cerebellar granule cells resulting from persistent activation of $GABA_A$ receptors. J Physiol 497:753–759.

Chao AC, Dix JA, Sellers MC, Verkman AS. 1989. Fluorescence measurement of chloride transport in monolayer cultured cells. Mechanisms of chloride transport in fibroblasts. Biophys J 56:1071–1081.

Curtis DR, Duggan AW, Felix D, Johnston GA. 1970. Bicuculline and central GABA receptors. Nature 228:676–677.

Deitmer JW, Rose CR. 2010. Ion changes and signalling in perisynaptic glia. Brain Res Rev 63:113–129.

Fahlke Ch, Kortzak D, Machtens JP. 2016. Molecular physiology of EAAT anion channels. Pflügers Arch 468:491–502.

Fairman WA, Vandenberg RJ, Arriza JL, Kavanaugh MP, Amara SG. 1995. An excitatory amino-acid transporter with properties of a ligand-gated chloride channel. Nature 375:599–603.

Gagnon KB, Adragna NC, Fyffe RE, Lauf PK. 2007. Characterization of glial cell K-Cl cotransport. Cell Physiol Biochem 20:121–130.

Gagnon KB, Delpire E. 2013. Physiology of SLC12 transporters: Lessons from inherited human genetic mutations and genetically engineered mouse knockouts. Am J Physiol Cell Physiol 304:C693–714.

Gensch T, Untiet V, Franzen A, Kovermann P, Fahlke Ch. 2015. Determination of intracellular chloride concentrations by fluorescence lifetime imaging. advanced time-correlated single photon counting applications. Springer Series in Chemical Physics 111:189–211.

Grosche J, Kettenmann H, Reichenbach A. 2002. Bergmann glial cells form distinct morphological structures to interact with cerebellar neurons. J Neurosci Res 68:138–149.

Grosche J, Matyash V, Moller T, Verkhratsky A, Reichenbach A, Kettenmann H. 1999. Microdomains for neuron-glia interaction: parallel fiber signaling to Bergmann glial cells. Nat Neurosci 2:139–143.

Haas M, Forbush B III. 2000. The Na-K-Cl cotransporter of secretory epithelia. Annu Rev Physiol 62:515–534.

Habela CW, Ernest NJ, Swindall AF, Sontheimer H. 2009. Chloride accumulation drives volume dynamics underlying cell proliferation and migration. J Neurophysiol 101:750–757.

Hoegg-Beiler MB, Sirisi S, Orozco IJ, Ferrer I, Hohensee S, Auberson M, Godde K, Vilches C, de Heredia ML, Nunes V, et al. 2014. Disrupting MLC1

and GlialCAM and ClC-2 interactions in leukodystrophy entails glial chloride channel dysfunction. Nat Commun 5:3475.

Holmseth S, Dehnes Y, Huang YH, Follin-Arbelet VV, Grutle NJ, Mylonakou MN, Plachez C, Zhou Y, Furness DN, Bergles DE, et al. 2012. The density of EAAC1 (EAAT3) glutamate transporters expressed by neurons in the mammalian CNS. J Neurosci 32:6000–6013.

Jensen AA, Fahlke Ch, Bjorn-Yoshimoto WE, Bunch L. 2015. Excitatory amino acid transporters: recent insights into molecular mechanisms, novel modes of modulation and new therapeutic possibilities. Curr Opin Pharmacol 20: 116–123.

Kahle KT, Rinehart J, Lifton RP. 2010. Phosphoregulation of the Na-K-2Cl and K-Cl cotransporters by the WNK kinases. Biochim Biophys Acta 1802:1150–1158.

Kanaka C, Ohno LK, Okabe A, Kuriyama K, Itoh T, Fukuda A, Sato K. 2001. The differential expression patterns of messernger RNAs encoding K-Cl cotransporters (KCC1,2) and Na-K-2Cl cotransporter (NKCC1) in the rat nervous system. Neuroscience 104:933–946.

Kaneko H, Putzier I, Frings S, Kaupp UB, Gensch T. 2004. Chloride accumulation in mammalian olfactory sensory neurons. J Neurosci 24:7931–7938.

Karus C, Mondragao MA, Ziemens D, Rose CR. 2015. Astrocytes restrict discharge duration and neuronal sodium loads during recurrent network activity. Glia 63:936–957.

Kettenmann H, Backus KH, Schachner M. 1987. gamma-Aminobutyric acid opens Cl^--channels in cultured astrocytes. Brain Res 404:1–9.

Kimelberg HK. 1981. Active accumulation and exchange transport of chloride in astroglial cells in culture. Biochim Biophys Acta 646:179–184.

Kimelberg HK, Macvicar BA, Sontheimer H. 2006. Anion channels in astrocytes: Biophysics, pharmacology, and function. Glia 54:747–757.

Kirischuk S, Kettenmann H, Verkhratsky A. 2007. Membrane currents and cytoplasmic sodium transients generated by glutamate transport in Bergmann glial cells. Pflügers Arch 454:245–252.

Komuro H, Yacubova E, Yacubova E, Rakic P. 2001. Mode and tempo of tangential cell migration in the cerebellar external granular layer. J Neurosci 21:527–540.

Kovalchuk Y, Garaschuk O. 2012. Two-photon chloride imaging using MQAE in vitro and in vivo. Cold Spring Harb Protoc 2012:778–785.

Ku HH. 1996. Notes on the Use of Propagation of Error Formulas. J Res Natl Bur Stand 70C:263–273.

Langer J, Rose CR. 2009. Synaptically induced sodium signals in hippocampal astrocytes in situ. J Physiol 587:5859–5877.

Lee M, McGeer EG, McGeer PL. 2011. Mechanisms of GABA release from human astrocytes. Glia 59:1600–1611.

Lehre KP, Danbolt NC. 1998. The number of glutamate transporter subtype molecules at glutamatergic synapses: Chemical and stereological quantification in young adult rat brain. J Neurosci 18:8751–8757.

Lehre KP, Levy LM, Ottersen OP, Storm-Mathisen J, Danbolt NC. 1995. Differential expression of two glial glutamate transporters in the rat brain: Quantitative and immunocytochemical observations. J Neurosci 15:1835–1853.

Luhmann HJ, Fukuda A, Kilb W. 2015. Control of cortical neuronal migration by glutamate and GABA. Front Cell Neurosci 9:4.

Machtens JP, Kortzak D, Lansche C, Leinenweber A, Kilian P, Begemann B, Zachariae U, Ewers D, de Groot BL, Briones R, et al. 2015. Mechanisms of anion conduction by coupled glutamate transporters. Cell 160:542–553.

MacVicar BA, Tse FW, Crichton SA, Kettenmann H. 1989. GABA-activated Cl^- channels in astrocytes of hippocampal slices. J Neurosci 9:3577–3583.

Makara JK, Rappert A, Matthias K, Steinhauser C, Spat A, Kettenmann H. 2003. Astrocytes from mouse brain slices express ClC-2-mediated Cl^- currents regulated during development and after injury. Mol Cell Neurosci 23:521–530.

Marandi N, Konnerth A, Garaschuk O. 2002. Two-photon chloride imaging in neurons of brain slices. Pflugers Arch 445:357–365.

Maus M, Cotlet M, Hofkens J, Gensch T, De Schryver FC, Schaffer J, Seidel CA. 2001. An experimental comparison of the maximum likelihood estimation and nonlinear least-squares fluorescence lifetime analysis of single molecules. Anal Chem 73:2078–2086.

Mercado A, Song L, Vazquez N, Mount DB, Gamba G. 2000. Functional comparison of the K^+-Cl^- cotransporters KCC1 and KCC4. J Biol Chem 275: 30326–30334.

Mongin AA. 2015. Volume-regulated anion channel-a frenemy within the brain. Pflügers Arch 3:421–441.

Mount DB, Mercado A, Song L, Xu J, George AL Jr, Delpire E, Gamba G. 1999. Cloning and characterization of KCC3 and KCC4, new members of the cation-chloride cotransporter gene family. J Biol Chem 274:16355–16362.

Muller T, Fritschy JM, Grosche J, Pratt GD, Mohler H, Kettenmann H. 1994. Developmental regulation of voltage-gated K^+ channel and $GABA_A$ receptor expression in Bergmann glial cells. J Neurosci 14:2503–2514.

Nehrke K, Arreola J, Nguyen HV, Pilato J, Richardson L, Okunade G, Baggs R, Shull GE, Melvin JE. 2002. Loss of hyperpolarization-activated Cl^- current in salivary acinar cells from *Clcn2* knockout mice. J Biol Chem 277:23604–23611.

Payne JA, Rivera C, Voipio J, Kaila K. 2003. Cation-chloride co-transporters in neuronal communication, development and trauma. Trends Neurosci 26:199–206.

Regan MR, Huang YH, Kim YS, Dykes-Hoberg MI, Jin L, Watkins AM, Bergles DE, Rothstein JD. 2007. Variations in promoter activity reveal a differential expression and physiology of glutamate transporters by glia in the developing and mature CNS. J Neurosci 27:6607–6619.

Richerson GB, Wu Y. 2003. Dynamic equilibrium of neurotransmitter transporters: Not just for reuptake anymore. J Neurophysiol 90:1363–1374.

Rivera C, Voipio J, Payne JA, Ruusuvuori E, Lahtinen H, Lamsa K, Pirvola U, Saarma M, Kaila K. 1999. The K^+/Cl^- co-transporter KCC2 renders GABA hyperpolarizing during neuronal maturation. Nature 397:251–255.

Robert SM, Sontheimer H. 2014. Glutamate transporters in the biology of malignant gliomas. Cell Mol Life Sci 71:1839–1854.

Rose CR, Ransom BR. 1996. Intracellular sodium homeostasis in rat hippocampal astrocytes. J Physiol 491: 291–305.

Saxena NC, Macdonald RL. 1996. Properties of putative cerebellar gamma-aminobutyric acid A receptor isoforms. Mol Pharmacol 49:567–579.

Shekarabi M, Salin-Cantegrel A, Laganiere J, Gaudet R, Dion P, Rouleau GA. 2011. Cellular expression of the K^+-Cl^- cotransporter KCC3 in the central nervous system of mouse. Brain Res 1374:15–26.

Shimamoto K, Sakai R, Takaoka K, Yumoto N, Nakajima T, Amara SG, Shigeri Y. 2004. Characterization of novel L-threo-beta-benzyloxyaspartate derivatives, potent blockers of the glutamate transporters. Mol Pharmacol 65:1008–1015.

Smith QR, Johanson CE, Woodbury DM. 1981. Uptake of 36Cl and 22Na by the brain-cerebrospinal fluid system: Comparison of the permeability of the blood-brain and blood-cerebrospinal fluid barriers. J Neurochem 37:117–124.

Staley K, Smith R, Schaack J, Wilcox C, Jentsch TJ. 1996. Alteration of $GABA_A$ receptor function following gene transfer of the CLC-2 chloride channel. Neuron 17:543–551.

Stölting G, Fischer M, Fahlke Ch. 2014. CLC channel function and dysfunction in health and disease. Front Physiol 5:378.

Su G, Kintner DB, Sun D. 2002. Contribution of Na^+-K^+-Cl^- cotransporter to high-$[K^+]_o$- induced swelling and EAA release in astrocytes. Am J Physiol Cell Physiol 282:C1136-C1146.

Torp R, Danbolt NC, Babaie E, Bjoras M, Seeberg E, Storm-Mathisen J, Ottersen OP. 1994. Differential expression of two glial glutamate transporters in the rat brain: an in situ hybridization study. Eur J Neurosci 6:936–942.

Untiet V, Moeller LM, Ibarra-Soria X, Sanchez-Andrade G, Stricker M, Neuhaus EM, Logan DW, Gensch T, Spehr M. 2016. Elevated cytosolic Cl^- concentrations in dendritic knobs of mouse vomeronasal sensory neurons. Chem Senses 8:669–676.

van Beugen BJ, Gao Z, Boele HJ, Hoebeek F, De Zeeuw CI. 2013. High frequency burst firing of granule cells ensures transmission at the parallel fiber to purkinje cell synapse at the cost of temporal coding. Front Neural Circuits 7:95.

Verkman AS. 1990. Development and biological applications of chloride-sensitive fluorescent indicators. Am J Physiol 259:C375-C388.

Wadiche JI, Amara SG, Kavanaugh MP. 1995. Ion fluxes associated with excitatory amino acid transport. Neuron 15:721–728.

Walz W, Mukerji S. 1988. KCl movements during potassium-induced cytotoxic swelling of cultured astrocytes. Exp Neurol 99:17–29.

Watase K, Hashimoto K, Kano M, Yamada K, Watanabe M, Inoue Y, Okuyama S, Sakagawa T, Ogawa S, Kawashima N, et al. 1998. Motor discoordination and increased susceptibility to cerebellar injury in GLAST mutant mice. Eur J Neurosci 10:976–988.

Winter N, Kovermann P, Fahlke Ch. 2012. A point mutation associated with episodic ataxia 6 increases glutamate transporter anion currents. Brain 135:3416–3425.

Yamada K, Watanabe M. 2002. Cytodifferentiation of Bergmann glia and its relationship with Purkinje cells. Anat Sci Int 77:194–108.

Yamada K, Fukaya M, Shibata T, Kurihara H, Tanaka K, Inoue Y, Watanabe M. 2000. Dynamic transformation of Bergmann glial fibers proceeds in correlation with dendritic outgrowth and synapse formation of cerebellar Purkinje cells. J Comp Neurol 418:106–120.

Yan Y, Dempsey RJ, Sun D. 2001. Expression of Na^+-K^+-Cl^- cotransporter in rat brain during development and its localization in mature astrocytes. Brain Res 911:43–55.

Yuasa S. 1996. Bergmann glial development in the mouse cerebellum as revealed by tenascin expression. Anat Embryol (Berl) 194:223–234.

Zhou Y, Danbolt NC. 2013. GABA and Glutamate Transporters in Brain. Front Endocrinol (Lausanne) 4:165.

Zhuo L, Sun B, Zhang CL, Fine A, Chiu SY, Messing A. 1997. Live astrocytes visualized by green fluorescent protein in transgenic mice. Dev Biol 187:36–42.

Zifarelli G, Pusch M. 2012. A kick-start for CLC antiporters' pharmacology. Chem Biol 19:1358–1359.

Zomot E, Bendahan A, Quick M, Zhao Y, Javitch JA, Kanner BI. 2007. Mechanism of chloride interaction with neurotransmitter: Sodium symporters. Nature 449:726–730.